Verification of numerical models for seismic fluid-structure-interaction analysis of advanced reactors

Conference Paper · August 2019

CITATIONS
4

READS
384

6 authors, including:

Ching-Ching Yu
University at Buffalo, The State University of New York
16 PUBLICATIONS **37** CITATIONS
SEE PROFILE

Faizan Ul Haq Mir
University at Buffalo, The State University of New York
9 PUBLICATIONS **8** CITATIONS
SEE PROFILE

Micheal Cohen
TerraPower
6 PUBLICATIONS **14** CITATIONS
SEE PROFILE

Justin Coleman
Idaho National Laboratory
50 PUBLICATIONS **143** CITATIONS
SEE PROFILE

Transactions, SMiRT-25
Charlotte, NC, USA, August 4-9, 2019
Division V

VERIFICATION OF NUMERICAL MODELS FOR SEISMIC FLUID-STRUCTURE-INTERACTION ANALYSIS OF ADVANCED REACTORS

Ching-Ching Yu[1], Faizan Ul Haq Mir[2], Michael Cohen[3], Justin L. Coleman[4], Philippe M. Bardet[5] and Andrew S. Whittaker[6]

[1] Doctoral Student, Department of Civil, Structural, and Environmental Engineering, University at Buffalo, Buffalo, NY 14260, USA (cyu23@buffalo.edu)
[2] Doctoral Student, Department of Civil, Structural, and Environmental Engineering, University at Buffalo, Buffalo, NY 14260, USA
[3] Mechanical Design Manager, TerraPower, Bellevue, WA 98008, USA
[4] Seismic Research Group Lead, Idaho National Laboratory, Idaho Falls, ID 83402, USA
[5] Associate Professor, Department of Mechanical and Aerospace Engineering, The George Washington University, Washington, D.C. 20052, USA
[6] SUNY Distinguished Professor and MCEER Director, Department of Civil, Structural, and Environmental Engineering, University at Buffalo, Buffalo, NY 14260, USA

ABSTRACT

The seismic design and qualification of advanced nuclear reactors and their internal components will rely on numerical models accommodating three-directional seismic inputs. If a reactor is subjected to extreme earthquake shaking, the responses of the contained fluid will be nonlinear, including sloshing and disengagement from the inner surfaces of the vessel, none of which can be calculated analytically. Numerical models for FSI analysis need to be first verified and validated before being used for seismic design and qualification of advanced reactors. A numerical model can be verified by comparing analysis results with analytical solutions and validated using data from physical testing. This paper describes 1) prior analytical work on seismic FSI analysis of base-supported cylindrical tanks, 2) analytical solutions accommodating head-supported cylindrical tanks with boundary conditions and geometries similar to prototype liquid metal reactor vessels, and 3) verification of numerical models for base- and head-supported cylindrical tanks prepared using the Arbitrary Lagrangian and Eulerian solver in LS-DYNA.

INTRODUCTION

Fluid-structure-interaction (FSI) analysis for seismic design and qualification of advanced nuclear reactors will rely on numerical models accommodating three-directional seismic inputs. There are no analytical solutions for FSI responses that can fully accommodate the seismic interaction of a reactor vessel and its internal components, and the effects of simultaneous input motions in the three directions. If a reactor is subjected to extreme earthquake shaking, the response of the fluid will be nonlinear, including sloshing and disengagement from the walls and the base of the tank, none of which can be calculated analytically.

Numerical models for FSI analysis need to be first verified and validated before being used for seismic design and qualification of advanced reactors and other nuclear reactors that contain a large volume of fluid (e.g., pressurized water and boiling water reactors). Numerical models can be verified by comparing analysis results with those generated using analytical solutions. A verified numerical model can be validated using data from physical testing. Yu (in progress) is developing verified and validated models for seismic FSI analysis of advanced reactors. The numerical models are analyzed using the Arbitrary Lagrangian and Eulerian (ALE) and the Incompressible Computational Fluid Dynamics (ICFD) solvers in LS-DYNA

(Livermore Software Technology Corporation (LSTC) 2017), both capable of calculating nonlinear FSI responses. The numerical models have been verified using the analytical solutions developed by Yu and others (e.g., Jacobsen (1949); Veletsos (1984); Chung and Chen (1977)). Validation of the verified models will be performed using data from earthquake simulator tests of a 1/10th-scale, base-supported, cylindrical tank, fabricated from carbon steel and filled with water. The tests are planned for Q2 and Q3 of 2019 at the University at Buffalo. This paper presents a part of the verification study performed in Yu. The preparation for the earthquake simulator tests is presented in a companion paper (Mir et al. 2019).

The numerical model presented in this paper is analyzed using the ALE solver in LS-DYNA and targeted to calculate fluid responses similar to those of the 1/10th-scale, base-supported, cylindrical tank prepared for the earthquake simulator tests. The dimensions used in the numerical models are identical to those of the 1/10th-scale test tank: a radius R of 0.79 m, a height H_s of 2 m, and a wall thickness h of 5 mm. The geometries of the test tank are loosely based on the prototype liquid metal reactors shown in Figure 1. Estimated using the equations given in Veletsos (1984)[1], the first impulsive frequency of the test tank ranges from about 100 Hz (full tank, fluid height $H = 2$ m) to 600 Hz (almost empty tank, $H = 0.2$ m), and the first convective frequency is about 0.77 Hz, which is insensitive to H. The test tank is very stiff based on its first impulsive frequency, and so the model of the tank is constructed with a rigid material. Two boundary conditions are considered in the analysis: 1) base-supported, which is consistent with the tank for the earthquake simulator tests, and 2) head-supported, which is used for advanced reactor vessels.

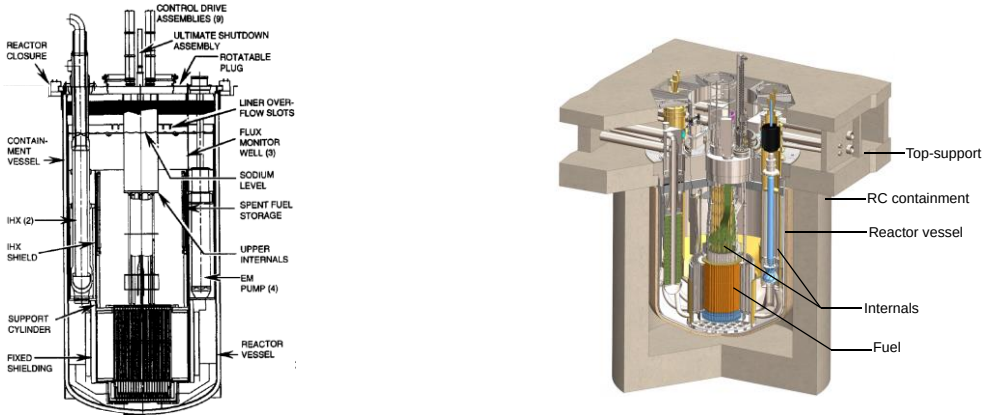

a. Gluekler (1997) b. adapted from TerraPower (2018)

Figure 1. Prototype liquid metal reactors, each of which includes a head-supported cylindrical tank, internal components, and a liquid metal coolant.

The numerical model of the base-supported tank is verified using the analytical solutions developed by Jacobsen (1949) and Veletsos (1984). The assumptions made to the analytical solutions must be consistently applied to the numerical model: 1) rigid tank filled with an ideal fluid, 2) unidirectional, horizontal seismic motion of a small amplitude, and 3) decoupling of the responses of the tank and its internal components. The solutions of Jacobsen and Veletsos are extended in this paper to accommodate head-supported tanks, and the numerical model of the head-supported tank is verified using these newly developed analytical solutions.

ANALYTICAL SOLUTIONS

The seismic FSI response of a tank subjected to unidirectional horizontal seismic motion of a small amplitude can be parsed into an impulsive and a convective component. The impulsive response is generated by the part of the fluid rigidly attached to and moving with the wall of the tank. The impulsive response disregards fluid waves and assumes the pressure on the initial free surface (i.e., open surface of

[1] The impulsive and convective frequencies are calculated using Eqs. (7-51) and (7-8) in Veletsos (1984), respectively.

the fluid at rest) to be zero as atmospheric pressure is not considered. The convective response is generated by the part of the fluid assumed theoretically *not* to move with the tank horizontally but to oscillate vertically. The vertical oscillation is a wave action that induces vertical displacements of the free surface. The convective response considers the pressures generated by wave actions, and together with the impulsive response completes the *hydrodynamic pressures* in the tank generated by earthquake shaking.

Figures 2a and b illustrate FSI responses of a base-supported tank and a head-supported tank, respectively. The FSI responses are parsed into impulsive and convective components, presented in vertical cross sections through the tanks accelerating in the x direction. The fluid associated with the impulsive response is attached to the inner surfaces (i.e., wall and base) of the base-supported or head-supported tanks and generates impulsive pressures, p_{imp}, on these surfaces. The impulsive pressures are balanced by reactions at the support, namely, at the base of the base-supported tank or at the top of the head-supported tank. The impulsive shear force, F_{imp}, in the x direction at the support (i.e., base or top) balances the resultant force of the horizontal p_{imp} on the wall (orange arrows). The impulsive moment, M_{imp}, about the y axis balances the resultant moment at the center (i.e., red solid circles) of the base or top generated by both p_{imp} on the wall (orange arrows) and p_{imp} on the base (pink arrows). The fluid associated with the convective response oscillates vertically and generates waves on the free surface with a small displacement d_w. The wave action induces convective pressures, p_{con}, on the wall (green arrows) and the base (blue arrows). Similar to the impulsive responses, p_{con} on the wall and the base are mechanically equilibrated by reactions at the support of the tank (i.e., base or head), including F_{con} and M_{con} (counterparts of F_{imp} and M_{imp}, respectively). Note that the directions of the reactions presented in Figure 2 are defined based on the positive coordinates (i.e., F_{imp} and F_{con} along the positive x direction) and the right-hand rule (i.e., M_{imp} and M_{con} in the counterclockwise direction about the y axis) for reasons of consistency.

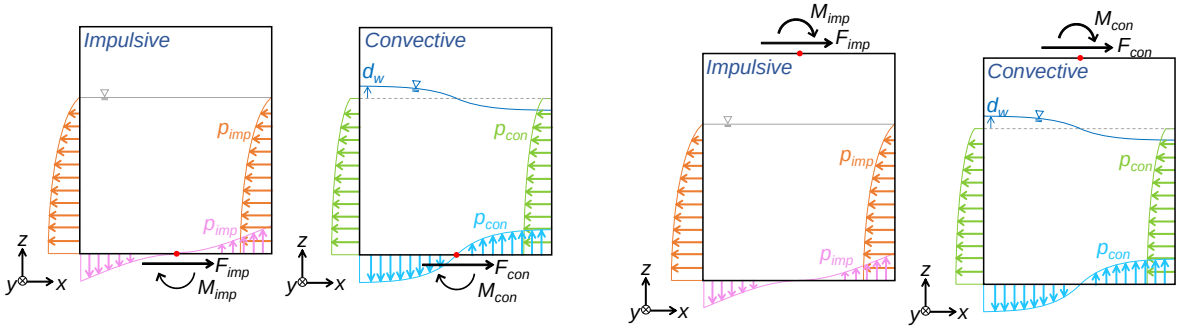

(a) base-supported (b) head-supported

Figure 2. FSI responses of base-supported tanks and head-supported tanks accelerating in the x direction, impulsive and convective components.

The analytical solutions used to verify the numerical model of the base-supported tank were derived by Jacobsen and Veletsos for the impulsive and the convective responses, respectively. These analytical solutions were derived based on the cylindrical coordinates (r, θ, z) shown in Figure 3, and the solutions were all functions of time, t. (Other information shown in Figure 3 will be presented and used in the section on results and verification.) Consequently, the results calculated using the solutions are response time series. The analytical solutions used to verify the numerical model of the head-supported tank are developed in this paper by extending the work of Jacobsen and Veletsos to accommodate the change in the boundary condition (i.e., from base-supported to head-supported).

Base-supported Tank

Jacobsen derived the analytical solutions of p_{imp}, F_{imp}, and M_{imp}. Veletsos decoupled each convective response into modal contributions and provided a solution for each mode. The solutions for convective responses in the jth mode ($j = 1, 2, \ldots$) included $p_{con,j}$, $F_{con,j}$, $M_{con,j}$, and $d_{w,j}$. Each convective response was the infinite algebraic sum of the corresponding modal responses (i.e., $j = 1$ to ∞). The derivations of

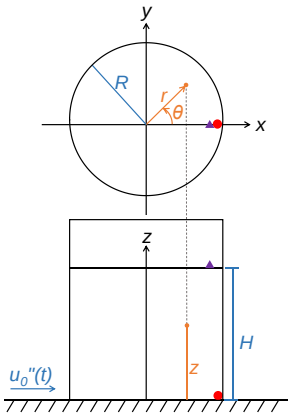

Figure 3: Cartesian coordinates and cylindrical coordinates shown on two cut-away views of a base-supported cylindrical tank, together with locations for reporting responses: hydrodynamic pressures at the red solid circle and vertical displacements of the free surface at the purple triangle.

the analytical solutions are not presented here but can be found in Yu (in progress) with corrections of the errors made in the original documents (i.e., Jacobsen and Veletsos). The impulsive and convective pressures on the wall of the tank (i.e., at $r = R$), $p_{imp,w}$ and $p_{con,w}$, along the vertical and the circumferential directions, z and θ, were:

$$p_{imp,w}(\theta,z,t) = -u_0''(t)\rho H \cos\theta \sum_{i=1}^{\infty} \frac{8(-1)^{i+1}}{\left[(2i-1)\pi\right]^2} \frac{I_1}{I_1'} \cos\left[(2i-1)\frac{\pi}{2}\frac{z}{H}\right] \tag{1}$$

$$p_{con,w}(\theta,z,t) = \sum_{j=1}^{\infty} p_{con,w,j} = \sum_{j=1}^{\infty} -A_j(t)\cdot \rho R \cos\theta \frac{2}{{n_j}^2 - 1} \frac{\cosh(n_j \frac{z}{R})}{\cosh(n_j \frac{H}{R})} \tag{2}$$

where ρ is the density of the fluid, $u_0''(t)$ is the input motion time series, I_1 is the modified Bessel function of the first kind with an order of 1 and a variable of $[(2i-1)\pi R / 2H]$, I_1' is the first derivative of I_1, n_j is a root (solution) of $J_1'(n_i) = 0$, and $A_j(t)$ is the acceleration time series in the jth convective mode, represented as a single-degree-of-freedom system with a convective frequency of $f_{con,j}$, subjected to the ground motion, $u_0''(t)$:

$$A_j(t) = \omega_{con,j} \int_0^t u_0''(\tau)\cdot \sin\omega_{con,j}(t-\tau)d\tau \tag{3}$$

$$\omega_{con,j} = 2\pi f_{con,j} = \sqrt{\frac{n_j g}{R}\tanh(n_j \frac{H}{R})} \tag{4}$$

where g is the gravitational acceleration. The impulsive and convective shear forces at the base of the tank in the x direction, F_{imp} and $F_{con,j}$, were:

$$F_{imp}(t) = u_0''(t) m_l \frac{H}{R} \sum_{i=1}^{\infty} \frac{16}{\left[(2i-1)\pi\right]^3} \frac{I_1}{I_1'} \tag{5}$$

$$F_{con}(t) = \sum_{j=1}^{\infty} F_{con,j} = \sum_{j=1}^{\infty} A_j(t)\cdot m_l \frac{R}{H} \frac{2}{n_j({n_j}^2 - 1)} \tanh(n_j \frac{H}{R}) \tag{6}$$

where m_l is the mass of the contained fluid. The impulsive and convective moments at the base of the tank about the y axis, M_{imp} and M_{con}, were:

$$M_{imp}(t) = u_0''(t) m_l \frac{H^2}{R} \sum_{i=1}^{\infty} \frac{16}{\left[(2i-1)\pi\right]^3} \frac{I_1}{I_1'} \left[1 - \frac{2(-1)^{i+1}}{(2i-1)\pi} + \frac{I_2}{I_1} (-1)^{i+1} \frac{R}{H} \right] \quad (7)$$

$$M_{con}(t) = \sum_{j=1}^{\infty} M_{con,w,j} = \sum_{j=1}^{\infty} A_j(t) m_l \frac{R^2}{H} \frac{2\tanh(n_j \frac{H}{R})}{n_j({n_j}^2 - 1)} \left[\frac{H}{R} - \frac{1}{n_j} \tanh(n_j \frac{H}{2R}) + \frac{J_2(n_j)}{J_1(n_j)} \frac{1}{\sinh(n_j \frac{H}{R})} \right] \quad (8)$$

where I_2 is the modified Bessel function of the first kind with an order of 2 and a variable of $[(2i-1)\pi R / 2H]$, and J_1 and J_2 are the Bessel function of the first kind with orders of 1 and 2, respectively. The vertical displacement of the free surface, d_w, along the radial and the circumferential directions, r and θ, was:

$$d_w(r,\theta,t) = \sum_{j=1}^{\infty} d_{w,j} = \sum_{j=1}^{\infty} -A_j(t) \cdot \frac{R}{g} \cos\theta \frac{2}{{n_j}^2 - 1} \frac{J_1(n_j \frac{r}{R})}{J_1(n_j)} \quad (9)$$

Head-supported Tank

With no deformation in the rigid wall, the impulsive and convective pressures in the tank are not affected by the location of the seismic input, whether at the base or the top. Consequently, the impulsive and convective shear forces at the top of the head-supported tank, which balances the horizontal resultant forces of the impulsive and convective pressures on the wall, respectively, are also identical to those at the base of the base-supported tank. The impulsive and convective moments at the support, M_{imp} and M_{con}, that balance the resultant moments generated by p_{imp} and p_{con}, respectively, are dependent on the location of the support (i.e., base or head) because of the change in the vertical distance (i.e., moment arm or lever arm) between the pressures and the support, which is moved from the base to the top. The analytical solutions of M_{imp} and M_{con} at the top of a head-supported tank about the y axis are:

$$M_{imp}(t) = u_0''(t) m_l \frac{H^2}{R} \sum_{i=1}^{\infty} \frac{16}{\left[(2i-1)\pi\right]^3} \frac{I_1}{I_1'} \cdot \left[-\frac{H_s}{H} + 1 - \frac{2(-1)^{i+1}}{(2i-1)\pi} + \frac{I_2}{I_1} (-1)^{i+1} \frac{R}{H} \right] \quad (10)$$

$$M_{con}(t) = \sum_{j=1}^{\infty} M_{con,w,j} = \sum_{j=1}^{\infty} A_j(t) m_l \frac{R^2}{H} \frac{2\tanh(n_j \frac{H}{R})}{n_j({n_j}^2 - 1)} \left[\frac{-H_s + H}{R} - \frac{\tanh(n_j \frac{H}{2R})}{n_j} + \frac{J_2(n_j)}{J_1(n_j)\sinh(n_j \frac{H}{R})} \right] \quad (11)$$

The derivations of M_{imp} and M_{con} can be found in Yu. Other responses that are identical to those of base-supported tanks are not repeated.

INPUT MOTIONS

Two sinusoidal motions time series, S-1 and S-2, presented in Figure 4, are used for the response-history analyses of the base- and head-supported tanks. To compare the analysis results to those calculated using the analytical solutions, identical assumptions for the input motion must be used. Accordingly, S-1 and S-2 are both small-amplitude, unidirectional, horizontal motions.

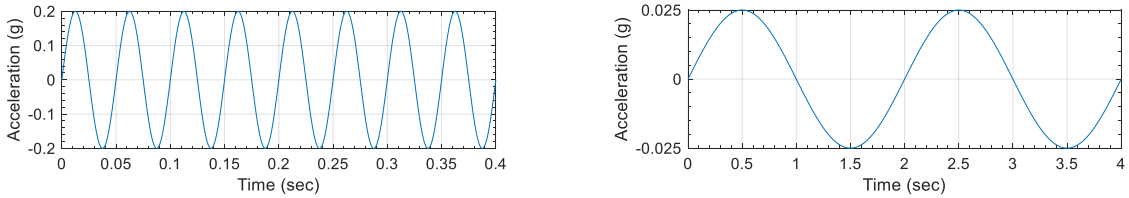

(a) S-1, PGA=0.2 g (b) S-2, PGA=0.025

Figure 4. Unidirectional, horizontal input motion time series for the response-history analyses of the tanks.

A typical, horizontal acceleration spectrum at a site in the U.S. generally has a peak value at the period of about 0.1 to 0.2 sec (i.e., frequency of 5 to 10 Hz), as shown in Figures 5a and b in the period and the frequency axes, respectively (according to the data from United States Geological Survey (2018)). The frequency of motion S-1 is chosen accordingly. To be consistent with the 1/10 length scale for the tank, the period scale of the spectrum is compressed by a factor of $\sqrt{10}$ (see the red lines in Figures 5), and the peak spectral acceleration is between periods of 0.03 and 0.06 sec after scaling, namely, at frequencies between 16 and 30 Hz. A frequency of 20 Hz is thereafter selected for motion S-1. The sinusoidal motion, S-2, is used for the purpose of driving the sloshing of the contained fluid. Accordingly, a frequency of 0.5 Hz is selected to be sufficiently close to the first convective frequency of the tank of 0.77 Hz. (A frequency of the sinusoidal motion greater than 0.5 Hz and closer to the first convective frequency could induce sloshing instability, for which numerical results cannot be verified by an analytical solution.) Input motion S-1 includes eight cycles of a 20-Hz sine wave with an amplitude (i.e., peak ground acceleration, PGA) of 0.2 g, and S-2 includes two cycles of a 0.5-Hz sine wave with an amplitude of 0.025 g. Motion S-2, which is expected to induce sloshing, uses a tiny PGA of 0.025 g to reduce the vertical accelerations of waves in the numerical models since the analytical solution (Veletsos) used herein for verification assumed this acceleration to be zero.

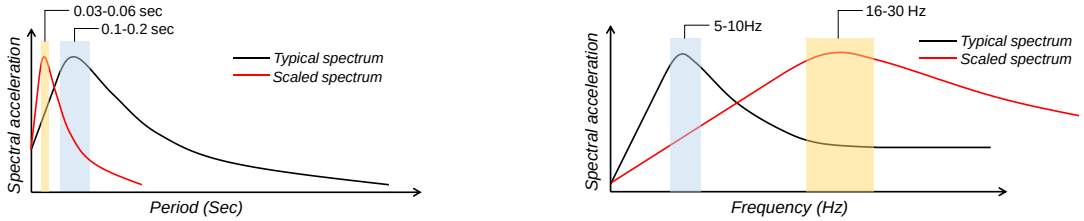

(a) period axis (a) frequency axis

Figure 5. Typical horizontal acceleration spectra and $1/\sqrt{10}$ th-scale acceleration spectra with respect to period.

NUMERICAL MODELS

Numerical models are constructed for the rigid cylindrical tank, with $R = 0.79$ m, $H_s = 2$ m, and, $h = 5$ mm, and filled with water to a height H of 1.2 m. With no deformation in the rigid tank, the responses of the contained fluid are not affected by the location of the support for horizontal seismic input, whether at the base or the head. Accordingly, one model is used for the analyses of the base- and head-supported tanks, but their support reactions are output at different locations (i.e., base or top). Figure 6 presents the numerical model for the responses-history analyses using the ALE solver, together with the global coordinates (x, y, z) consistent with those shown in Figure 3. Figures 6a and b present the finite elements for the tank filled with water to 1.2 m, topped by air, in the isometric view. The tank is shown in blue, the water is shown in yellow, and the air is shown in gray in the figures. The sizes of the elements shown in Figures 6a and b are optimized, resulting in smaller elements for the fluids (i.e., water and air) adjacent to the tank wall, around the boundary between the water and the air (i.e., free surface), and along the direction of the seismic input (i.e., x direction) across the diameter of the tank. The tank and the fluids (i.e., water and air) share nodes at their interface. In the model, 5732 Lagrangian, four-node, shell elements (i.e., quadrilateral elements) are used for the tank; 56928 Eulerian, eight-node, solid elements (i.e., brick elements) are used for the water; and 37952 Eulerian brick elements are used for the air. These Eulerian elements do not deform with the fluid; rather, they serve together as a grid in the fluid domain through which the fluid can flow. Integration points for calculating fluid responses are located in each grid cell (i.e., each Eulerian element). Accordingly, the Eulerian elements will not be distorted by the large deformation of the fluid. Figure 6c presents the meshless water domain, at the first step of the analysis (i.e., time $t = 0$).

The results of the numerical model for the base- and head-supported tanks are compared with the corresponding analytical solutions for hydrodynamic pressures, reactions at the support, and vertical displacements of the free surface. The analytical solutions addressed the support reactions associated with

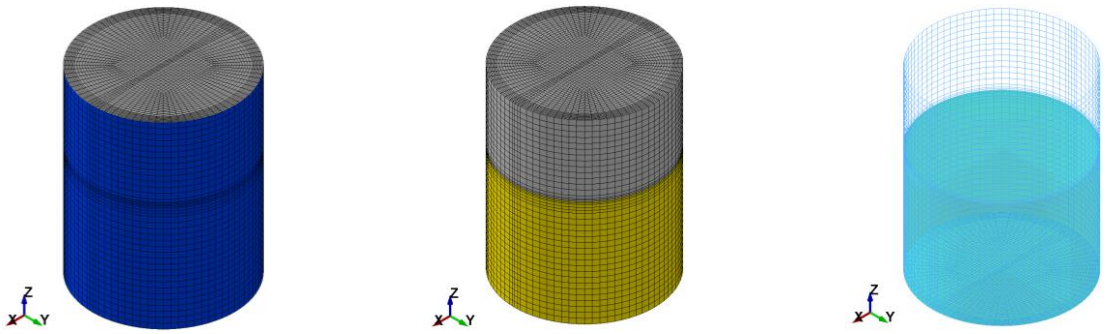

(a) tank and air (b) water and air (c) tank and water at $t = 0$

Figure 6. ALE models of a cylindrical tank with $R = 0.79$ m, $H_s = 2$ m, $h = 5$ mm, and $H = 1.2$ m.

hydrodynamic loadings and did not consider those associated with the inertial force of the tank. Accordingly, the inertial force of the tank in the numerical model must be removed to generate reactions consistent with those analytically calculated. The mass of the rigid tank is reduced by assigning a tiny density $\rho_s = 100$ kg/m^3 to the elements, significantly smaller than the common density of carbon steel (e.g., 8000 kg/m^3), which makes the inertial force of the tank negligible. Other mechanical properties consistent with carbon steel are assigned to the elements of the tank, including the elastic modulus E_s of 2×10^{11} N/m^2 and the Poisson's ratio υ_s of 0.25. These values do not affect the responses of the rigid tank but must be defined in the models. No damping is applied to the tank (i.e., damping ratio=0).

The analytical solutions were developed for ideal fluids, which are inviscid and incompressible. The water elements are assigned a density ρ_w of 1000 kg/m^3 and a viscosity μ_w of 0 to be inviscid. The bulk modulus K_w consistent with water, 2.15×10^9 N/m^2, is used for the model, which is sufficiently large to achieve incompressibility based on the results of a sensitivity analysis. The analytical solutions did not consider the effect of the atmospheric pressure on the FSI responses. Accordingly, the elements of the air are assigned *void properties* through the *INITIAL_VOID card for the model. The gravitational acceleration g of 9.81 m/s^2 is assigned to the z direction of the numerical models. The tank weighs 0.06 kN, the water weighs 23 kN, and the air is weightless.

RESULTS AND VERIFICATION

The results of the numerical model are compared with the analytical solutions for hydrodynamic pressures, reactions at the support, and vertical displacements of the free surface. Hydrodynamic pressures and reactions are parsed into impulsive and convective components, and vertical displacements of the free surface are associated with only convective components. It is not possible to separate the impulsive and convective components in the responses calculated using the numerical model. Accordingly, to compare the analytical and numerical results, the analytical solution of each impulsive response time series and that of the corresponding convective response time series are algebraically summed. The convective responses given in Eqs. (2), (6), (8), (9), and (11) are the algebraic sums of infinite modes (i.e., $j = 1$ to ∞) in the theory (Veletsos), but only the first ten modes (i.e., $j = 1$ to 10) are included in the calculation herein since the contributions of the eleventh and higher modes are negligible for the tank and the input motions used in the numerical model.

Base-supported Tank

The time series of the hydrodynamic pressures, p, calculated using the numerical models and the sum of Eqs. (1) and (2) are compared at the red solid circle on the tank presented in Figure 3. The red solid circle is at (x, y, z)=(0.79 m, 0, 0) on the Cartesian coordinate system used in the numerical model and at (r, θ, z)=(0.79 m, 0, 0) on the cylindrical coordinate system used in the analytical solutions. Figures 7a and b present the results for input motions S-1 and S-2, respectively.

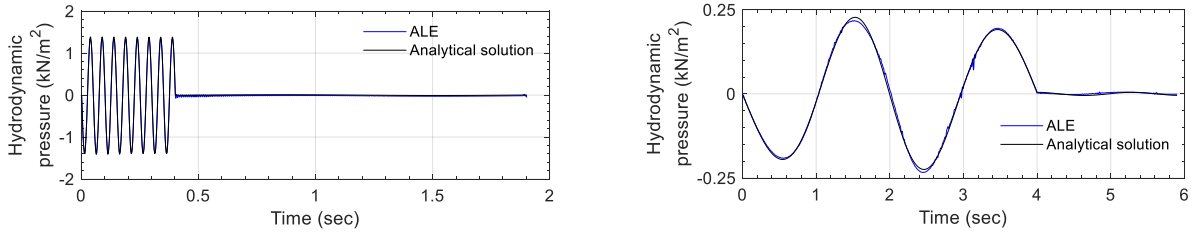

(a) S-1 (b) S-2

Figure 7. Time series of the hydrodynamic pressure at the red solid circle shown in Figure 3.

The time series of the shear force in the x direction, F, and the moment about the y axis, M, at the base of the tank calculated using the numerical model are compared with those calculated using in the corresponding analytical solutions. The sum of Eqs. (5) and (6) is the solution for F, and the sum of Eqs. (7) and (8) is the solution for M. Figures 8 and 9 present the results of F and M, respectively, for both input motions S-1 and S-2.

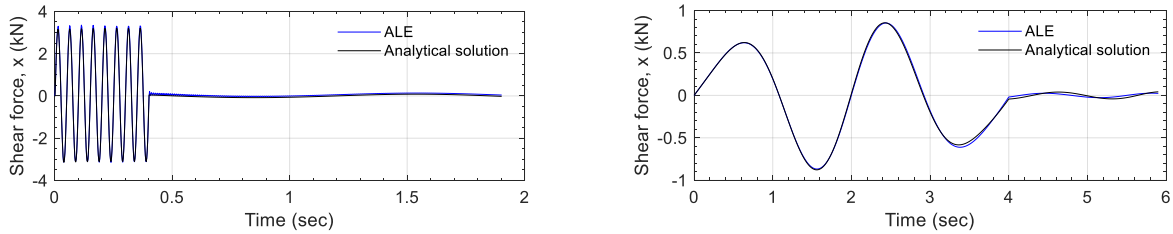

(a) S-1 (b) S-2

Figure 8. Time series of the shear force in the x direction at the base of the tank.

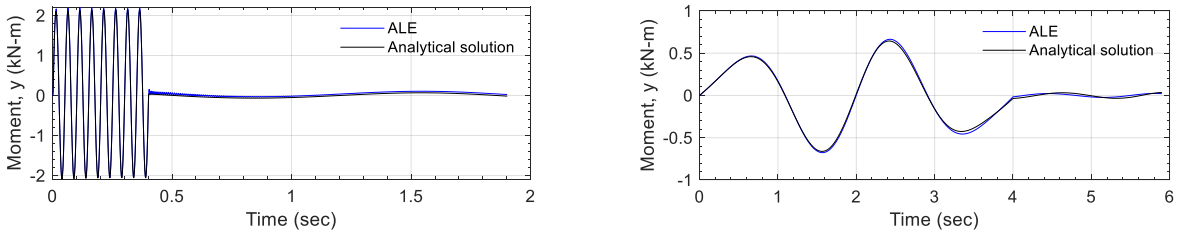

(a) S-1 (b) S-2

Figure 9. Time series of the moment about the y axis at the base of the tank.

The results of the numerical model and Eq. (9) are compared for the vertical displacements on the free surface, d_w, at the purple triangle shown in Figure 3. The purple triangle is a short distance of $0.1R$ (i.e., 8 cm) away from the wall of the tank because the position of the free surface at the interface between the fluid and the wall cannot be calculated accurately by the ALE solver due to the boundary effect (Do 2019). The coordinates of the purple triangle are at (x, y, z)=(0.71 m, 0, H) in the Cartesian system used in the numerical models and at (r, θ, z)=(0.71 m, 0, H) in the cylindrical system used in Eq. (9). Figures 11a and b present the vertical displacements of the free surface (i.e., wave height with respect to $z = H$) for motions S-1 and S-2, respectively.

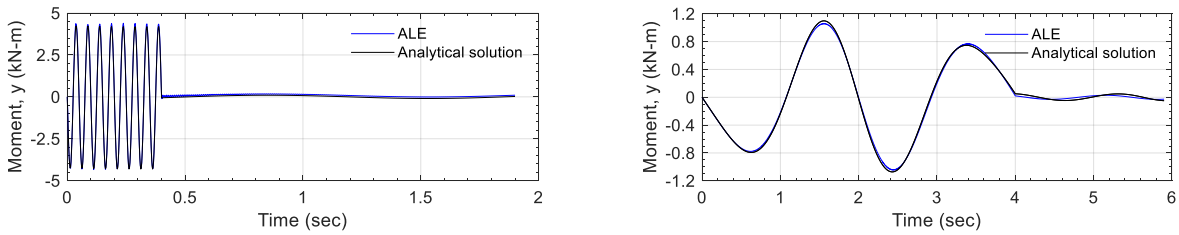

(a) S-1 (b) S-2

Figure 10. Time series of the moment about the y axis at the top of the head-supported tank.

Head-supported Tank

As noted in the section on analytical solutions, the hydrodynamic pressure and the shear force at the support of a head-supported tank are identical to those of a base-supported tank, but the moments at the supports of the two tanks are different. Consequently, only the moments about the y axis at the top of the head-supported tank calculated using the numerical model are compared here with those calculated using the sum of Eqs. (10) and (11), as shown in Figures 8a and b for motions S-1 and S-2, respectively.

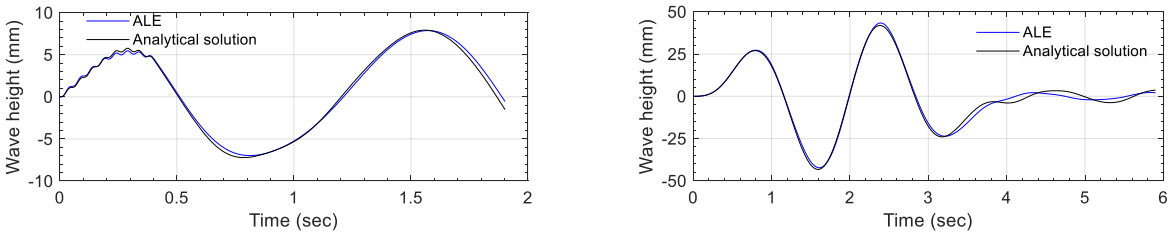

(a) S-1 (b) S-2

Figure 11. Time series of the wave height above $z = H$ at the purple triangle presented in Figure 3.

Discussion

To compare p, F, M, and d_w calculated using the numerical model and the analytical solutions, the percentage differences are calculated at the time steps of the peak responses in the histories for the analytical solutions shown in Figures 7 to 10. Accordingly, for the base-supported tank, the percentage differences in p, F, M, and d_w for motion S-1 are calculated at 0.0125, 0.0125, 0.0125, and 1.56 seconds, respectively. For the base-supported tank subjected to motion S-2, the percentage differences in p, F, M, and d_w are calculated at 2.45, 1.56, 1.56, and 1.59 seconds, respectively. For the head-supported tank, for which only the results of M are presented here, the percentage differences are calculated at 0.0125 and 1.56 seconds for motions S-1 and S-2, respectively. Table 1 presents the maximum responses and the percentage differences of the maximum responses of the numerical model with respect to the analytical solutions. The percentage differences are all less than 5%, which confirms that the numerical model of the rigid cylindrical tank is verified, for small-amplitude, unidirectional, horizontal seismic motions.

SUMMARY AND CONCLUSIONS

The seismic design and qualification of advanced nuclear reactors and their internal components will rely on verified and validated numerical models that can accommodate three-directional seismic inputs. This paper verifies a numerical model of a rigid cylindrical tank with dimensions and geometries identical to the 1/10-scale base-supported tank planned for earthquake simulator testing at the University at Buffalo. The geometries of this 1/10-scale test tank are loosely based on those of a prototype liquid metal reactor vessel.

The seismic FSI analyses of the numerical model are performed using the ALE solver in LS-DYNA. The input motions used in the analyses are 20-Hz and 0.5-Hz sinusoidal time series, both of which are small-amplitude, unidirectional, horizontal motions. Two boundary conditions are considered in the numerical model, base- and head-supported. The numerical results of the base-supported tank are compared with the analytical solutions developed by Jacobsen (1949) and Veletsos (1984). The numerical results of the head-supported tank are compared with the analytical solutions developed herein, extended from the work of Jacobsen and Veletsos. The percentage differences of the maximum FSI responses calculated using the numerical model and the analytical solutions are less than 5%, which enables the authors to conclude that the ALE model is verified, for rigid cylindrical tanks and small-amplitude, unidirectional, horizontal seismic motions. Other verification studies can be found in Yu (in progress), including numerical models for flexible tanks and internal components analyzed using both the ALE and ICFD solvers in LS-DYNA.

Table 1: Comparison of the maximum FSI responses calculated using the numerical model and the analytical solutions presented in Figures 7 to 10.

Motion	Response	Base-supported tank			Head-supported tank		
		Numerical model	Analytical solution	Difference (%)[1]	Numerical model	Analytical solution	Difference (%)[1]
S-1	p (kN/m^2)	1.4	1.4	0	--	--	--
	F (kN)	3.2	3.3	4	--	--	--
	M (kN-m)	2.1	2.1	2	4.3	4.3	0
	d_w (mm)	7.9	7.9	-1	--	--	--
S-2	p (kN/m^2)	0.22	0.23	4	--	--	--
	F (kN)	0.88	0.87	-1	--	--	--
	M (kN-m)	0.66	0.68	2	1.10	1.06	-1
	d_w (mm)	43.3	42.2	-2	--	--	--

1. Percentage difference of FSI responses calculated using the numerical model with respect to those calculated using the analytical solutions, to the nearest 1%

ACKNOWLEDGMENTS

The information, data, or work presented herein was funded in part by the Advanced Research Projects Agency-Energy (ARPA-E), U.S. Department of Energy, under Award Number DE-AR0000978, and in part by TerraPower and the U.S. Department of Energy under CRADA 14CR04. The views and opinions of the authors expressed herein do not necessarily state or reflect those of the United States Government or any agency thereof, or TerraPower.

REFERENCES

Chung, H., and Chen, S. (1977). "Vibration of a group of circular cylinders in a confined fluid." *Journal of Applied Mechanics*, 44(2), 213-217.

Do, I. (2019). Personal communication.

Gluekler, E. L. (1997). "U.S. advanced liquid metal reactor (ALMR)." *Progress in Nuclear Energy*, 31(1-2), 43-61.

Jacobsen, L. S. (1949). "Impulsive hydrodynamics of fluid inside a cylindrical tank and of fluid surrounding a cylindrical pier." *Bulletin of the Seismological Society of America*, 39(3), 189-204.

Livermore Software Technology Corporation (LSTC) (2017). "LS-DYNA keyword user's manual-Version R 10.0.", Livermore, CA.

Mir, F. U. H., Yu, C.-C., Cohen, M., Bardet, P., Coleman, J., and Whittaker, A. (2019). "Dataset generation for validation of fluid-structure interaction models." *Transactions, 25th International Conference on Structural Mechanics in Reactor Technology (SMiRT-25)*, Charlotte, NC.

TerraPower, Bellevue, WA. "TWR technology: preparing nuclear energy for global growth." <http://terrapower.com/technologies/twr>, accessed on July 4, 2018.

United States Geological Survey (USGS), Reston, VA. "Earthquake hazards program: unified hazard tool." <https://earthquake.usgs.gov/hazards/interactive/>, accessed on Dec 11, 2018.

Veletsos, A. (1984). "Seismic response and design of liquid storage tanks." *Guidelines for the seismic design of oil and gas pipeline systems*, Committee on Gas and Liquid Fuel Lifelines, American Society of Civil Engineers (ASCE), Reston, VA, 255-370.

Yu, C.-C. (in progress). "Verification and validation of numerical models for seismic fluid-structure-interaction analysis of liquid metal reactors." Thesis, presented to University at Buffalo, Buffalo, NY, in partial fulfillment of the requirements for the degree of Doctor of Philosophy.